Scanning array radar system for bridge subsurface imaging

Chieh-Ping Lai, Yu-Jiun Ren, Tzu Yang Yu

Chieh-Ping Lai, Yu-Jiun Ren, Tzu Yang Yu, "Scanning array radar system for bridge subsurface imaging," Proc. SPIE 8347, Nondestructive Characterization for Composite Materials, Aerospace Engineering, Civil Infrastructure, and Homeland Security 2012, 834713 (4 April 2012); doi: 10.1117/12.915647

SPIE.

Event: SPIE Smart Structures and Materials + Nondestructive Evaluation and Health Monitoring, 2012, San Diego, California, United States

Scanning Array Radar System for Bridge Subsurface Imaging

Chieh-Ping Lai*[a], Yu-Jiun Ren[a], and Tzu-Yang Yu[b]
[a]LR Technologies Inc., 511 Casey ln, Rockville, USA 20850;
[b]Dept. of Civil and Environment Engineering, University of Massachusetts Lowell, Lowell, MA USA 01854

ABSTRACT

Early damage detection of bridge has been an important issue for modern civil engineering technique. Existing bridge inspection techniques used by State Department of Transportation (DOT) and County DOT include visual inspection, mechanical sounding, rebound hammer, cover meter, electrical potential measurements, and ultrasonics; other NDE techniques include ground penetrating radar (GPR), radiography, and some experimental types of sensors. Radar technology like GPR has been widely used for the bridge structure detection with a good penetration depth using microwave energy. The system to be presented in this paper is a different type of microwave sensing technology. It is focus on the subsurface detection and trying to find out detail information at subsurface (10 cm) with high resolution radar imaging from a flexible standoff distance. Our radar operating frequency is from 8-12 GHz, which is different from most of the current GPR systems. Scanning array antenna system is designed for adjustable beamwidth, preferable scanning area, and low sidelobe level. From the theoretical analysis and experimental results, it is found that the proposed technique can successfully capture the presence of the near-surface anomaly. This system is part of our Multi-Modal Remote Sensing System (MRSS) and provides good imaging correlations with other MRSS sensors.

Keywords: Bridge subsurface, concrete, NDE, radar, array antenna, SAR, imaging, GPR.

1. INTRODUCTION

1.1 Background

Managing the growing population of deteriorated transportation infrastructure systems (i.e. highway bridges) and being able to accurately inspect them in a timely and cost effective manner is a major societal challenge within the United States today. Traditional nondestructive testing/inspection/evaluation (NDT/NDI/ NDE) methods for highway bridges cannot currently provide an accurate and rapid evaluation (independent of human biases and interpretation) on a routine basis to prevent deteriorated bridges from sudden collapse. Automated, low-cost, efficient bridge inspection techniques for interrogating critical bridge components are needed. Existing highway bridge inspection techniques include visual inspection, mechanical sounding, rebound hammer, cover meter, electrical potential measurements, and ultrasound which are typically time consuming, labor intensive, and cost inefficient. Safety issue, interference with existing traffic, and subjective evaluation of visual inspection are additional disadvantages in such inspections. The objective of this project is to develop a multi-modal remote sensing system (MRSS) that will be used as the next generation of rapid, distant, interrogation technology for bridge inspection. The proposed MRSS combines advantages of NDT (local inspection) and structural health monitoring (SHM) (global, continuous monitoring), using innovative continuous wave imaging radar (CWIR), digital image correlation (DIC), and fiber optic sensors (FOS) to deliver a cost-effective, robust solution for the inspection and monitoring of critical transportation infrastructure such as highway bridges. MRSS represents the next-generation of portable bridge inspection technology for efficient and time saving inspection, evaluation and rating of bridges.

1.2 Multi-modal Remote Sensing System

The proposed MRSS consists of (1) a portable integrated sensor component with continuous wave imaging radar (CWIR), optical cameras for digital image correlation (DIC), global positioning system (GPS), position sensors, and laser ranger for in-situ inspection, and (2) a fiber optics sensor (FOS) component for continuous monitoring. Figure 1

Nondestructive Characterization for Composite Materials, Aerospace Engineering, Civil Infrastructure, and Homeland Security 2012, edited by Andrew L. Gyekenyesi, Tzu-Yang Yu, Peter J. Shull, Aaron A. Diaz, H. Felix Wu,
Proc. of SPIE Vol. 8347, 834713 · © 2012 SPIE · CCC code: 0277-786X/12/$18 · doi: 10.1117/12.915647

illustrates the installation and operation of MRSS for detecting surface anomalies (e.g., surface cracking in concrete, surface rust of steel). MRSS will allow inspectors to:

i) Monitor structural behavior using fiber optic sensors (FOS),
ii) Scan different locations on bridge girders and piers from a stationary position using continuous wave imaging radar (CWIR) in a short period of time,
iii) Detect surface changes (bulging, cracking, stress/strain) using digital image correlation (DIC), and
iv) Synergize the multi-modal measurements collected by radar, high-resolution camera, and fiber optic sensors. In this presentation, we will focus on the development of the CWIR.

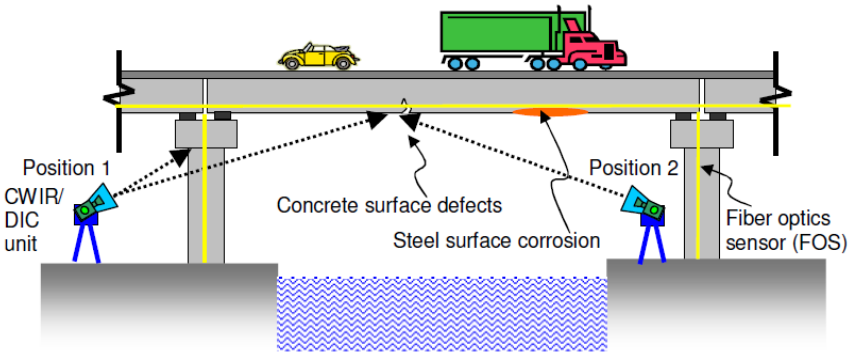

Figure 1. Inspection and monitoring scheme of the proposed MRSS technology.

2. SURFACE AND SUBSURFACE SENSING USING CW IMAGING RADAR

2.1 System architecture

In this work, a new CWIR is developing to detect the surface cracking and deterioration of highway bridges by utilizing surface electromagnetic (EM) reflections collected by the portable imaging radar. Subsurface imaging and damage detection is achieved by processing reflection measurements at different frequencies, relative elevations, inspection angles, and signal polarizations, using synthetic aperture radar (SAR) algorithms. Possible frequency bands to be explored are X-band (8-12 GHz), Ku-band (12-18 GHz), S-band (2-4 GHz), and C-band (4-8 GHz). Figure 2 shows the surface scanning scheme of CWIR on a reinforced concrete highway bridge as an example.

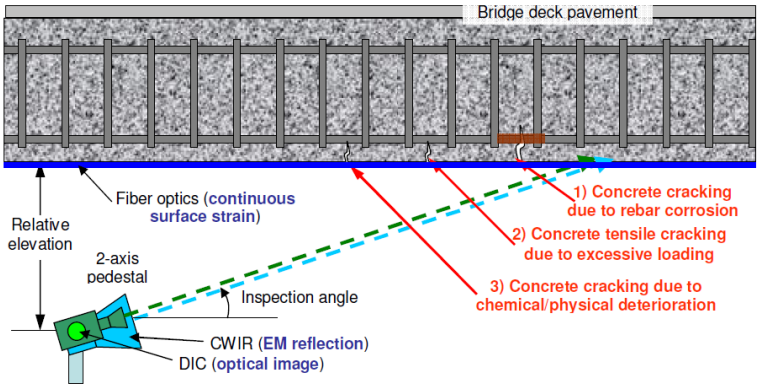

Figure 2. Inspection and monitoring scheme of MRSS on a bridge structure.

The design purpose of the prototype instrument is to validate the dual-polarization bridge detection and mitigation through X-band radar (8-12 GHz). X-band operation is selected because of the commercially available transmitters, components, and antennas for their relatively small size, and low costs. The design can be transported to other bands if desired. The system needs to have low-cost, light weight, and possess scalability. Transmission-reflection (T-R) phase

coherency is not required because only non-Doppler operations are supported. However, phase and amplitude coherency within all receive channels are required. The aperture size limitations of the suggested portable sensor platform confine the angular resolution to about 10°.

The important aspect of the proposed design is scalability of the transceiver system. A wideband X-band FMCW (frequency modulated continuous wave) radar transmitter is used as the basis of the transmit system. The minimum system in this design employs analog beamformers to output one horizontally polarized and one vertically polarized analog channel, while the array aperture can support from 4×4 to 8×8 independent dual-pol. (H-polarization and V-polarization) channels if desired. Beam steering relies on the mechanical rotary stage in this design and also the SAR imaging algorithms, like Stripmap SAR or Spotmap SAR, but advanced beamforming can also be supported by modifying the beamforming structures.

2.2 Data process flow

Figure 3 shows the proposed data processing flow of CWIR. Before operation, the radar system must be calibrated in-lab with small-size calibration targets. The timing cycle of the radar starts from power-up of the transmitter. Synchronization between the transmit trigger and the scan angle will ensure the data acquisition starts when the angle is stabilized and a transmit signal has been sent. At each angle, return signals are sampled according to range gate setting and the desired surveillance range. The transmit wideband FMCW signal are sent in H-/V-polarizations and the return signals are received in H-pol. or V-pol. channels, depending on command. This configuration enables the calculation of three variables: reflectivity, differential reflectivity and differential phase. In Figure 4, the proposed operation of CWIR is a spotlight SAR mode where the collected returned signals at different radar positions can be integrated to form spatial images. It has been reported that post-processing techniques can reveal the presence and location of subsurface defects in multi-layer concrete structures and for the detection of reinforced bars [1]. Figure 5 shows a concrete cylinder wrapped by fiberglass sheet and its reconstructed images using returned radar signals collected at a distance more than 30 meters in laboratory. Long-range measurements were made possible by the use of two reflectors in laboratory.

With a pre-designed, continuous bandpass filter, the rate of image reconstruction processing can be accelerated to only a few seconds. Performance of radar signals with different polarizations (e.g., transverse electric (TE), transverse magnetic (TM)) will be also investigated and integrated to form polarimetric SAR images for damage detection. Advantages of the proposed distant radar sensing and imaging technique over other existing methods include: i) large-area sensing using a flexible inspection distance, ii) effective inspection by optimal combinations of sensing mode, frequency, distance, angle, and signal polarization for different types of defect and damage, iii) data visualization by SAR operations and back-projection algorithms, iv) efficient inspection by two types of inspection (preliminary/broad and detailed). In the proposed CWIR, damage detection will be conducted at two levels; raw returned signal and reconstructed image. This innovation provides us with flexibility in the interpretation of results for inspection.

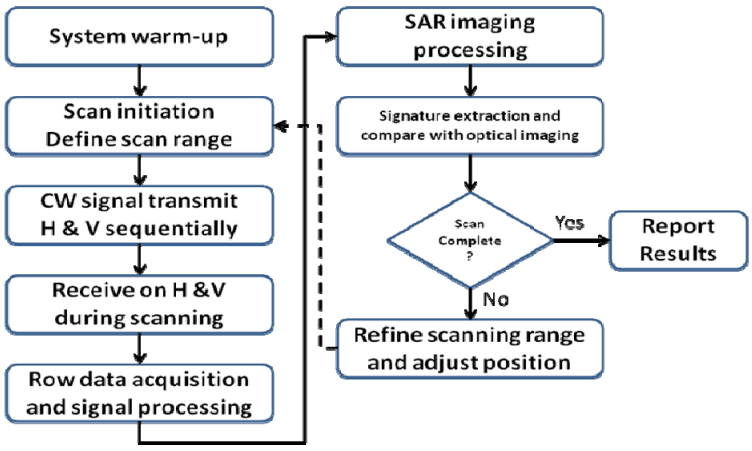

Figure 3. System data processing flow of CWIR.

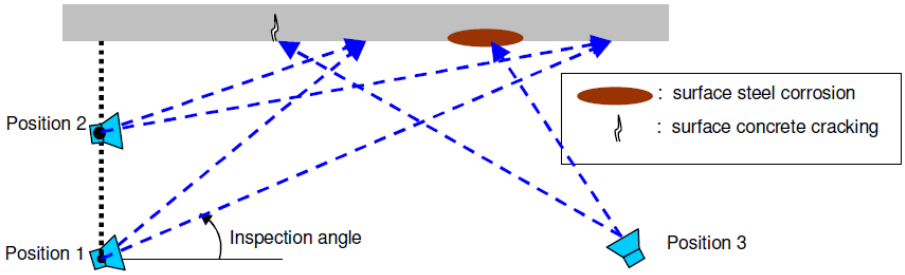

Figure 4. SAR operation for signals focusing.

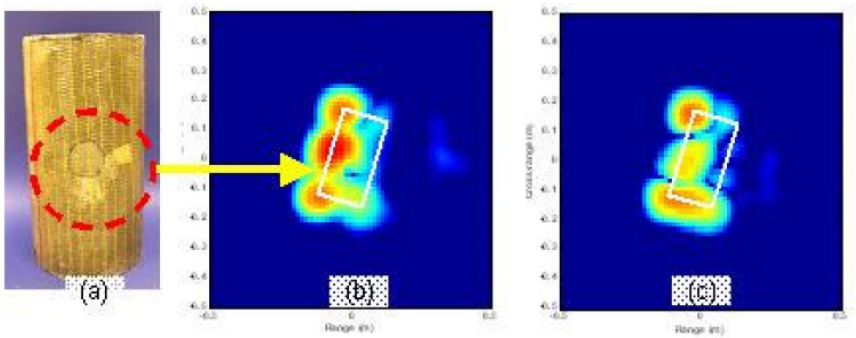

Figure 5. (a) Fiberglass-concrete cylinder; (b) reconstructed image of damaged side; and (c) reconstructed image of intact side.

2.3 Radar system

In order to build up capability of the lab measurement system for radar imaging, a 2D X-Z positioner is designed to integrate with our sensing equipment. X-Z system utilizing the HZR belt driven unit for the vertical axis. The rigidity of the HZR permits higher vertical speed, greater X-axis acceleration, and larger moment loading. The lab measurement system will include the X-Z positioner, two wideband antennas for Transmit (TX) and Receive (RX), power amplifier, low noise amplifier and Network analyzer. We will place the target sample 1-meter in front of the sensor system then scan through alone X axis (0-4 meter) and Z axis (0-1.5 meter). Figure 6 explains the setup of Lab measurement system. The data collected in the lab will be S21 data format and they will be processed using Matlab in order to get SAR imaging. The data we get from the lab measurement system will be compared to the data generated by our simulation modeling.

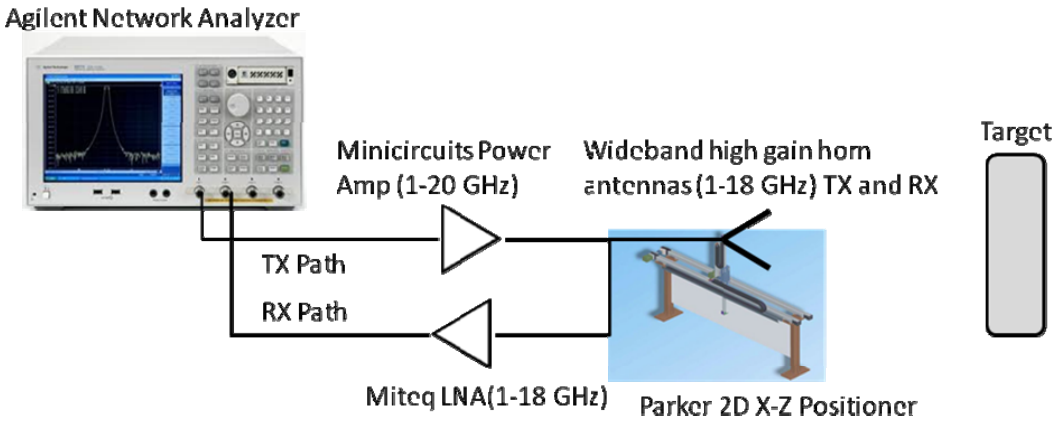

Figure 6 Lab measurement system.

The prototype system is different than the Lab measurement. The goal of the final deliverable design is a portable and low cost system. The expensive network analyzer will be replaced to a FMCW transceiver which has a customized frequency and bandwidth based on the imaging results from the lab measurement system. This type of FMCW radar system has already been used for dielectric material measurement and SAR imaging research. There are some recent published papers using similar system design as our concept. Those systems already work well but they are very bulky. Our system will be more mature and has advanced software control functions. Figure 7 shows the system diagram of our final system and you can see most of the hardware can be reused from the lab measurement system. RF amplifiers, TX/RX antennas and 2-D positioner are the same as the lab measurement system. So the lab system and final system will still be correlated based on similar hardware components.

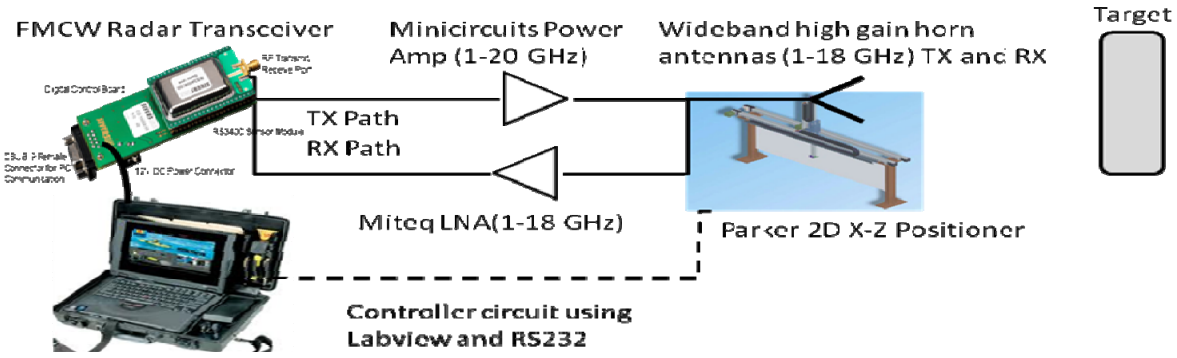

Figure 7 Radar imaging system prototype.

The final system specification is list in Table 1. The maximum detection range is varied and depends on the transmit power of transceiver and resolution requirements. For the radar simulation efforts, we choose simulation parameters from available components and device in order to compare with later experimental data.

Table 1. Design parameters of the CWIR.

Range	1 m to 50 m
Range Resolution	Better than 3 cm
Angular Resolution	~5 degree
Weight	60 lbs
Dimensions	18 × 12 × 6 inch^3
Power Consumption	TBD
Data Update Rate	2s per scan map (±60° azimuth; PRF = 2.5 kHz, 50 integrations)
Transmitter	Solid-state modulator driving device
Transmit Antenna	Horns (H-pol. and V-pol.)
Frequency	8 GHz -12 GHz
Wavelength	~3 cm
RF Front end Bandwidth	4000 MHz
Transmit Peak Power	0.5 W
Transmit Antenna Gain	15 dBi
Receiver	
Receive Antenna	Double Ridged Horn
Receiver Noise Figure	2 dB
Receiver Bandwidth	~2 MHz
Antenna Gain	15 dBi

3. RCS ANALYSIS OF THE BRIDGE CONCRETES

RCS characteristic of the detecting targets, i.e., various concretes and rebars, is the major performance parameter of the radar system. The RCS information assists to process the radar imaging which affects the hardware requirement and radar resolution. According to the six cylindrical specimens provided by the UML, we have finished the RCS simulation within 2-18 GHz. With this broad bandwidth, it helps understand their radiation characteristics. Based on the given information, these six specimens can be grouped into three, as shown in Figure 8. The description of specimens is provided as the following, where the specimens' materials used in the simulation are summarized in Table 2.

(1) Concrete cylinder: diameter 4 inch and height 8 inch, along with two Styrofoam balls. One 2 inch diameter ball had been placed at central axis of cylinder when the center of the ball was 2.65 inch above from the base, and another 1" diameter Styrofoam ball had been placed at central axis of cylinder, when the center of the ball was 2.65 inch below from the top. The mix 4 design of concrete was cement: sand: gravels = 1:2:3 (by weight), and the water to cement ratio was 0.55 (by weight).
(2) Concrete cylinder: diameter 4 inch and height approximately 8 inch, was cast along with Styrofoam box (0.5"X0.5"X4") impurity. The Styrofoam slice had been embedded at the center of cylindrical surface of the cylinders. Again the mix proportion was cement: sand: stone chips = 1:2:3, water cement ratio 0.55.
(3) Cement mortar cylinder: diameter 4 inch and height 7.9 inch. Mix proportion was selected 1:2 = cement: sand and water cement ratio was 0.5.
(4) Concrete cylinder: diameter 4 inch and height 7.9 inch. Mix proportion of concrete was selected, cement: sand: stone chips = 1:2: 3, and water/cement ratio was 0.5.
(5) Cement paste cylinder: diameter 4 inch and height 8 inch, was cast.
(6) Concrete cylinder: diameter 4 inch and height 7.65 inch, with #4 rebar at the center. Mix proportion of concrete was selected, cement: sand: stone chips = 1:2: 3, and water/cement ratio=0.55.

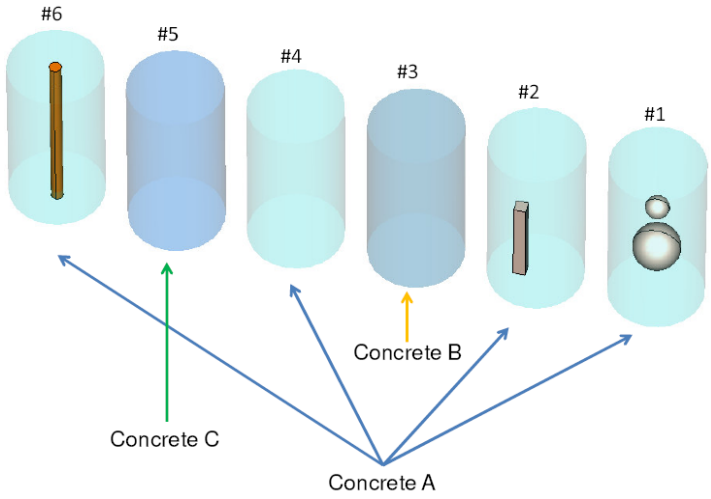

Figure 8. Concrete specimens prepared by the UML (the right first is assigned as #1, and the left one is #6). Group A: #1, #2, #4, and #6; Group B: #3; Group C: #5.

The RCS values of those specimens with the incidence angle (θ, ϕ) at (0, 0) and (90, 90) degrees have been obtained using a 3-D electromagnetic simulator. The values at (0, 90) are similar those at (90, 90) due to the symmetry of the specimens. The RCS is highly dependent on the geometry/shape of the target and especially the incidence angle. It can be observed that the trend of the RCS magnitude is similar at the same angle. Within 2-18 GHz, the RCS is between -15 to -45 dBsm. Within the X-band, the RCS is relative stable and the variation is about 5-10 dB. Figure 9 shows the 3-D RCS patterns at 10 GHz. The concrete itself can be considered as a dielectric material. Therefore, without any metal inserted its RCS value is smaller than most of the metal objects. For a PEC cylinder structure, the RCS can be expressed by

$$\sigma_{max} = \frac{2\pi r h^2}{\lambda}$$

From this equation, if the cylinder is long (higher) and a signal with a shorter wavelength is used, then we are able to obtain a larger RCS. The height of these specimens are only 8 inch (= 20.32 cm) that is much less than 1 meter and affects the RCS. Since Specimen #6 looks close to the concrete with the rebar generally used, we show its RCS at different frequencies in Figure 10. In general, the maximum RCS increase with the frequency, matched to the equation shown above.

Table 2. Material properties of the concrete cylinder (Specimens #1, #2, #4, #6)

Concrete mix portion (cement : sand : stone chips/ gravels)= 1:2:3	
Water cement ratio = 0.55	
Electric property	
Permittivity (F/m): 4.88 @ 1GHz	Dielectric dispersion (loss tangent): 0.011
Permeability (H/m^2): 1	Conductivity (S/m): 0.017
Mechanic property	
Material density (kg/m^3): 2393.84	Young's modulus (GPa): 30
Thermal expansion coefficient (1/K): 12X10^{-6}	Poisson's ratio: 0.2
Thermal property	
Thermal conductivity (W/K/m): 0.4-0.7	Heat capacity (kJ/K/kg): 0.75-0.88
Thermal diffusivity (m^2/s): 66	

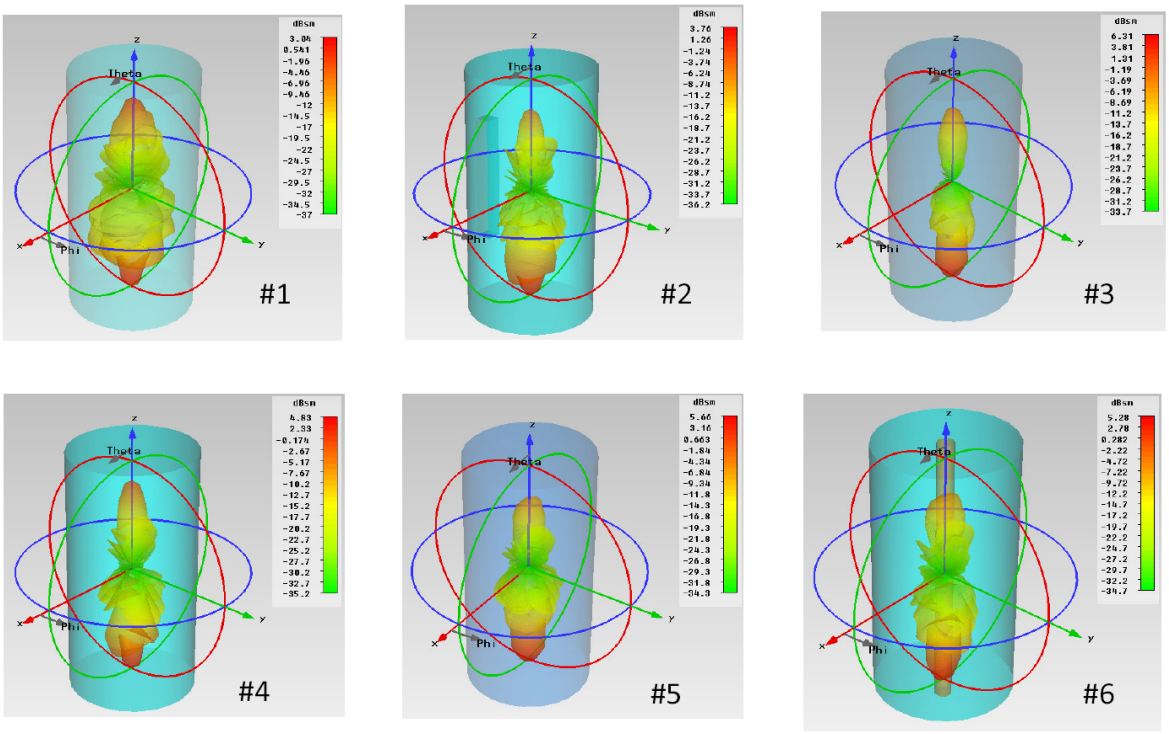

Figure 9. RCS patterns of all specimens at 10 GHz (unit: dBsm).

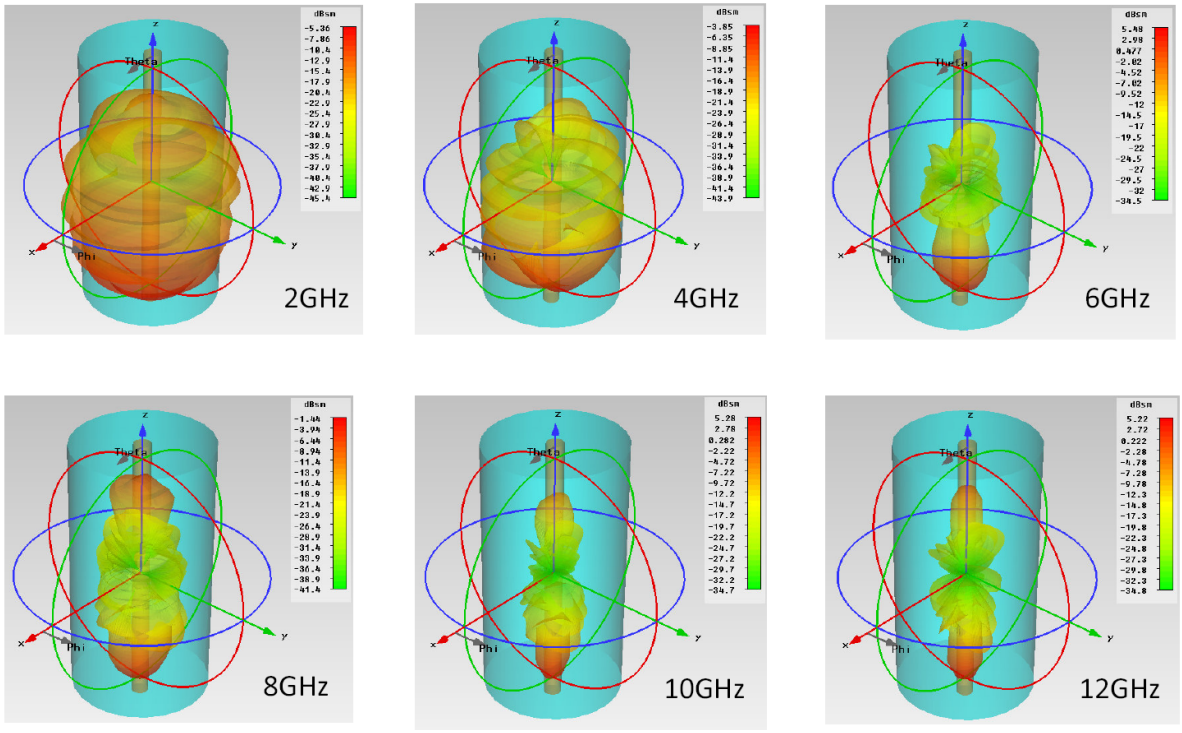

Figure 10. RCS patterns of Specimen #6 at 2, 4, 6, 8, 10, and 12 GHz (unit: dBsm).

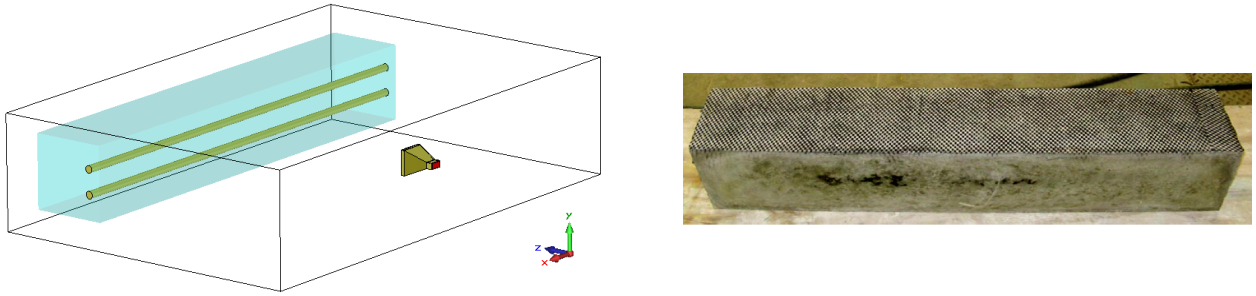

Figure 11. Environment to emulate the SAR analysis. The concrete specimen is 91 cm (3 ft) long and two No. 4 bars are inserted. The distance between the specimen and the horn antenna is 50 cm. A photo of the reinforced concrete beam is shown.

4. EM FIELDS AND SAR

The goal of this radar system design is to inspect the structure health of the bridge through the CW radar SAR imaging. The RCS is one important parameter which especially impacts the transmitting power, low noise amplifier, and the antenna system. The SAR imaging will be the final results to be presented. To verify the concept of our system, it's able to use a 3-D electromagnetic simulator to emulate the transmitting and reflected signals which will be used as the input raw data for the signal processing.

RC beam specimen has been prepared for the mechanical and DIC testings. Starting from this specimen, we used it as the reference target for the SAR analysis. This 3-foot long rectangular concrete has two #4 rebars inside and the antenna is the horn antenna introduced in the previous section. The simulation environment is shown in Figure 11 where the frequency range is 8-12 GHz ($\Delta f = 20$ MHz) and the sampling number is 201 points. The short pulse signal and Gaussian signal are two good choices to start with, as the input signal of the SAR imaging. Figure 12 shows an example of the

input/output Gaussian signals through the horn antenna. The waveform (period) is decided by the bandwidth and the sampling points, in which the magnitude is normalized to one.

To compare the difference with the concretes consisted of different materials, we use the same volume as the RC beam specimen to fill with (a) pure concrete and (b) concrete with the rebar, and check the electromagnetic field distribution on different cutting planes and also the echoes from these two objects while the antenna is in the center position. The electromagnetic field will propagate through the object which looks like ripples in each cut, as shown in Figure 13. The information useful for the radar signal processing is the echo signals from the object. Due the different materials, it will give different time-domain characteristics (reflection echo), which can be used for the SAR imaging. Figure 14 shows the electromagnetic field distribution of the concrete with rebars. It's required to collect data of time- and frequency-domains to verify the imaging algorithm which is under the developing process.

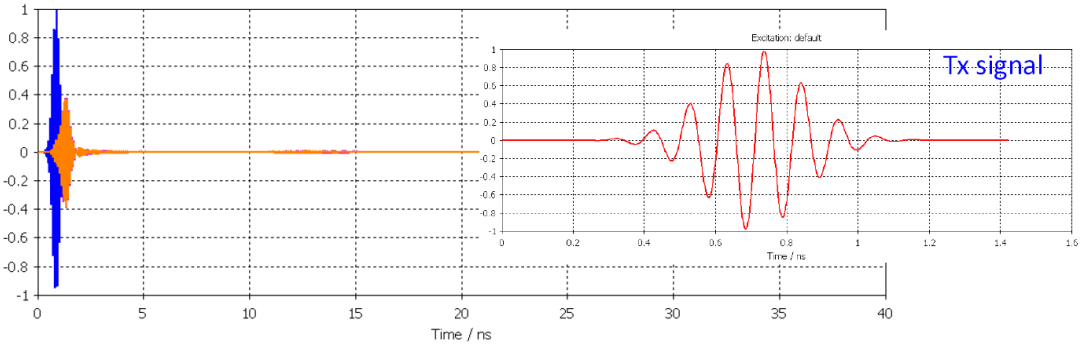

Figure 12. Time signal at the horn antenna: blue line is the input (transmit) signal and the orange line is the output (receive) signal. Detailed input signal is shown in the inset.

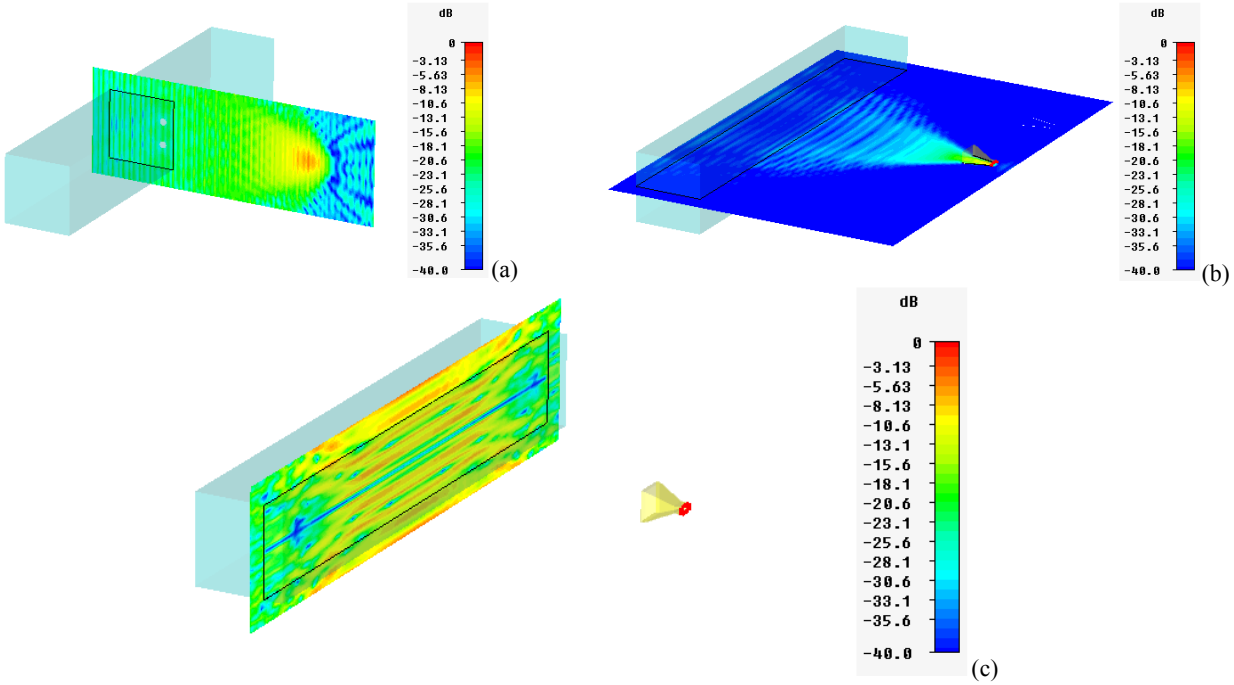

Figure 13. The E-field distributions on the different planes: (a) X-plane, (b) Y-plane, and (c) Z-plane, when the specimen is fully filled with the concrete.

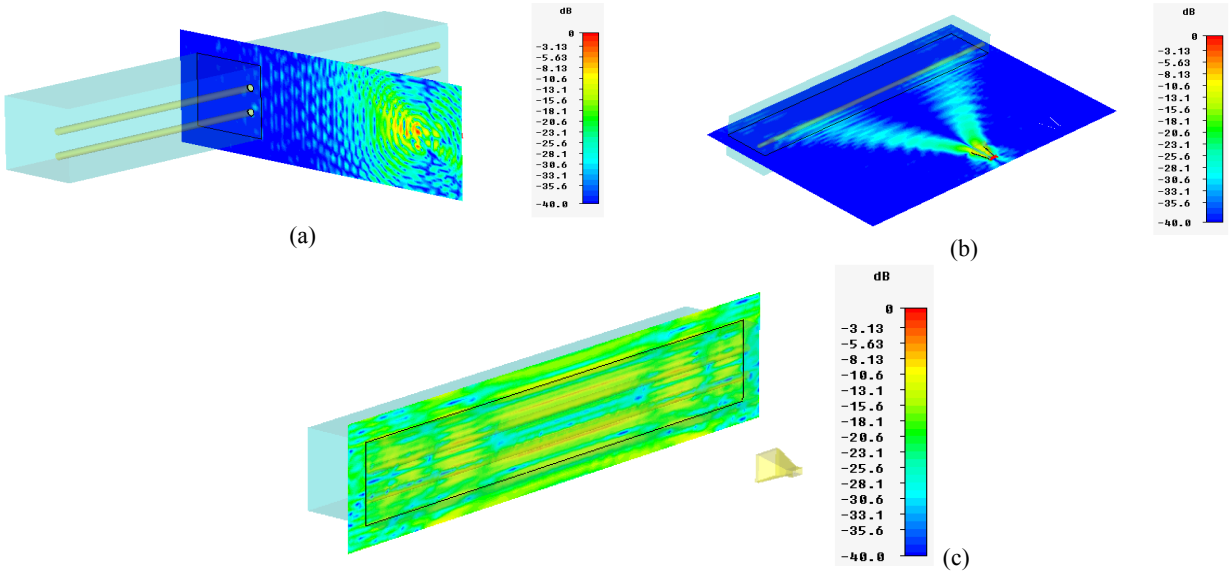

Figure 14. The E-field distributions on the different planes: (a) X-plane, (b) Y-plane, and (c) Z-plane, when the concrete specimen includes two #4 reinforced bars.

5. FUTURE WORKS

So far, we have finished the initial radar system design and are integrating the hardware and the control algorithm. A laboratory system for concept verification and data collection is under processing while various specimens are ready to be test. Some of them have been analyzed with the RCS and SAR as mentioned above. The numerical simulation model which can predict the reflection and scattering of sample target signals will be developed to understand the theoretical properties of the concretes, which can generate the associated RCSs for the RC beam specimen sample. Three dimensional SAR images will be obtained and used to inspect the targeted infrastructure systems. All of them will be verified through experimental data with the bridges in the state of Massachusetts.

6. CONCLUSIONS

The final product of this Phase III research project will be an integrated sensing system with both NDT (CWIR and DIC) and SHM (FOS) components. This development will serve as a paradigm for long-term bridge maintenance and a platform to combine the technical benefits of conventional NDT and SHM technologies for Remote Sensing and Spatial Information applications. While the emphasis of application is for bridges, the proposed MRSS can also be applied to tunnels, roadways, and buildings.

ACKNOWLEDGEMENTS

This work is partially supported by the U.S. DOT Research and Innovative Technologies Administration (RITA) Commercial Remote Sensing & Spatial Technologies (CRS&SI) under Grant RITAS-11-U-UML. The authors want to thank the U.S. DOT RITA for funding this project.

REFERENCES

[1] Yu, T-Y, Distant damage assessment method for multi-layer composite systems using electromagnetic waves, *Journal of Engineering Mechanics*, ASCE, 137 (8): 547-560 (2011).
[2] Skolnik, M. I., [Radar Handbook], Second Edition, McGraw-Hill, Boston & New York, Chap.21 (1990).
[3] Oppenheim, A. V., Willsky, A. S., and Nawab, S. H., [Signals & Systems], Second Edition, Prentice Hall, Upper Saddle River, New Jersey, (1996).